Journal of Non-Crystalline Solids 650 (2025) 123378

Contents lists available at ScienceDirect

Journal of Non-Crystalline Solids

journal homepage: www.elsevier.com/locate/jnoncrysol

# Pressure-driven structural evolution of amorphous InN

Murat Durandurdu

*Department of Materials Science and Nanotechnology Engineering, Abdullah Gül University, Kayseri, Türkiye*

ARTICLE INFO

*Keywords:*
Amorphous
Indium nitride
Polyamorphism
Crystallization

ABSTRACT

Through constant-pressure ab initio simulations, we have uncovered high-pressure phase transformations in amorphous indium nitride for the first time. Our results reveal a distinct two-step progression under compression. Initially, a polyamorphic transition occurs, where the low-density amorphous (LDA) phase transforms into a high-density amorphous (HDA) phase. This HDA structure remains stable in some pressure range and then crystallization initiates, leading to a rocksalt configuration. Upon decompression, the HDA phase reverts to an amorphous network with a slightly higher density and coordination number than the initial LDA state.

## 1. Introduction

Indium nitride (InN) stands out as a promising semiconductor material due to its unique properties, including a small effective electron mass, high carrier mobility, high saturation velocity, and narrow bandgap [1–5]. These attributes make InN ideal for high-performance applications in electronics, such as high-electron mobility transistors, optoelectronic devices, and highly efficient solar cells [6–8]. However, producing high-quality InN thin films through epitaxial growth presents significant challenges.

In contrast to crystalline InN, amorphous InN (a-InN) might offer an alternative material that may bypass some of these challenges. Amorphous materials, due to their simpler fabrication processes, can be easier to produce and can offer advantages such as lower cost and flexibility. So, a-InN might be a promising alternative to crystalline InN, with potential in electronic devices akin to thin-film III-nitrides such as AlN and GaN. In response, some efforts have been directed toward the synthesis and characterization of a-InN thin films [9,10]. Ab initio simulations [11] have provided detailed structural insights, indicating that a-InN is chemically ordered with an average coordination number of about 4.0. Unlike crystalline InN, however, a-InN includes unique structural motifs—specifically edge-sharing tetrahedra—that do not appear in the crystalline form, underscoring the distinctive bonding environment of the amorphous phase.

Under ambient conditions, InN crystallizes in the hexagonal wurtzite (WZ) structure and it undergoes a structural transition to a rocksalt (RS) phase at about 10–13 GPa, accompanied by a substantial volume collapse of approximately 17–20 %. [12–14] Recently, high-pressure cycling studies at 20 GPa reported amorphization of InN [15].

While the high-pressure response of WZ-InN is well-documented, the behavior of a-InN under similar conditions is not yet entirely understood. In this work, we examine the high-pressure behavior of a-InN through ab initio constant-pressure simulations, providing new insights into its structural evolution and stability under compression.

## 2. Method

We employed an ab initio technique [16] with a local density approximation through the Ceperley and Alder functional [17] as parameterized by Perdew and Zunger [18] to study high-pressure simulations on a-InN. Troullier-Martins pseudopotentials [19] were used, with In 3d states treated as core electrons. Simulations were conducted under constant pressure using the NPH ensemble with the power quenching technique. The electronic structure was represented with double zeta plus polarization (DZP) basis sets, and Brillouin zone sampling was limited to the Γ point. Pressure adjustments were executed via the Parrinello-Rahman method [20], with structural relaxation continued until the maximum atomic force was below 0.01 eV/Å. Due to the structural similarities between a-AlN and a-InN, we based the generation of our a-InN model on an established a-AlN configuration [21]. After performing relaxation, the resulting structure aligned well with previously reported data on a-InN [11].

## 3. Results

The equation of state (EOS) for a-InN, as illustrated in Fig. 1, reveals two significant volume collapses, each corresponding to a first-order phase transition. Initially, the volume decreases gradually under

*E-mail address:* murat.durandurdu@agu.edu.tr.

https://doi.org/10.1016/j.jnoncrysol.2024.123378
Received 20 November 2024; Received in revised form 15 December 2024; Accepted 19 December 2024
Available online 24 December 2024

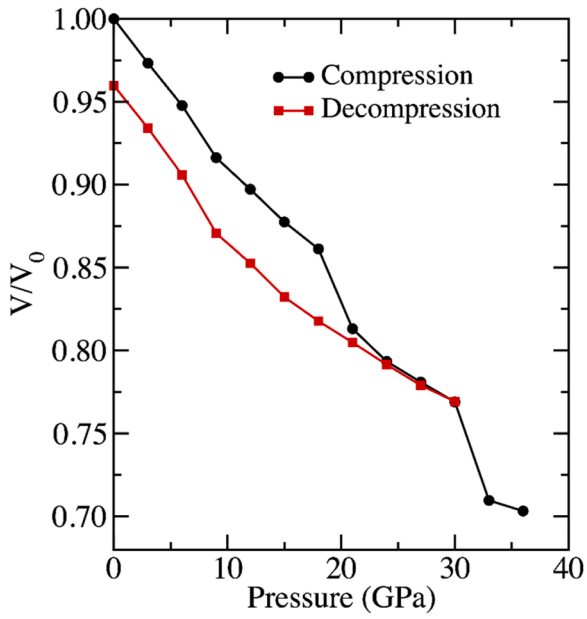


**Fig. 1.** The EOS of a-InN exhibits two volume collapses at 21 GPa and 33 GPa, corresponding to first-order phase transitions. A hysteresis loop upon pressure release from 30 GPa, just before the second collapse, shows partial volume recovery, with the final structure having a density approximately 4 % higher than the initial state.

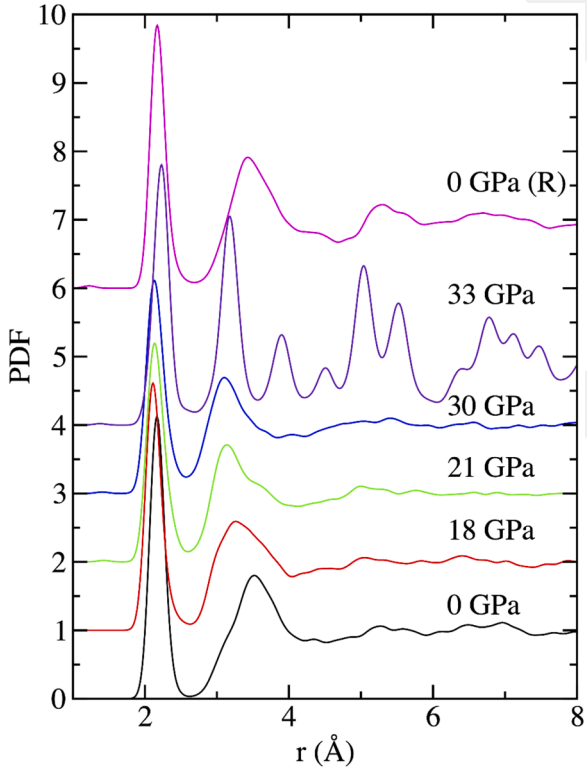


**Fig. 2.** Total pair distribution function (PDF) of a-InN at various pressures.

compression until a pronounced collapse occurs at 21 GPa. Upon further compression, the volume continues to decrease steadily until a second marked collapse is observed at 33 GPa. These findings indicate that a-InN undergoes two distinct first-order phase transitions at these pressure points.

To monitor pressure-induced changes, we first use pair distribution function (PDF) analysis (Fig. 2), revealing that a-InN maintains its amorphous nature up to 33 GPa. At this pressure, distinct long-range correlations emerge, marking a shift toward a more ordered structure. Visual examination of the structure at 33 GPa (Fig. 3) using the VESTA program [22] suggests the onset of crystallization; however, structural defects and coordination irregularities prevent clear symmetry identification. Drawing on high-pressure behavior observed in WZ-InN, we postulate that this high-pressure phase may adopt an imperfect RS structure.

Since the material remains amorphous up to 33 GPa, the transition accompanied by a large volume collapse at 21 GPa likely represents an amorphous-to-amorphous transformation, specifically a shift from a low-density amorphous (LDA) to a high-density amorphous (HDA) phase, a phenomenon identified as polyamorphism. This interpretation is reinforced by coordination number analysis: as shown in Fig. 4, the coordination numbers gradually rise between 6 and 18 GPa, followed by a sharp increase to 4.7 at 21 GPa, consistent with an LDA-to-HDA transition. Further compression of the HDA phase raises progressively the coordination number and a sudden jump to approximately 6.0 at 33 GPa.

Additional insights into these transitions are provided by coordination distribution analysis, shown in Fig. 5. At ambient pressure, both In and N atoms have an average coordination number of 4.027, with 90 % of In and 94 % of N atoms in fourfold coordination. The remaining atoms show either threefold or fivefold coordination (3.3 % of In and 1.85 % of N are threefold; 6.5 % of In and 4.62 % of N are fivefold), consistent with previous models [11]. Around 6 GPa, fivefold coordination begins to increase. In the HDA phase, approximately 60 % of In atoms exhibit fivefold coordination, with around 7 % showing sixfold coordination; the rest remain fourfold coordinated. For N atoms, about 51 % display fivefold and 12 % sixfold coordination, while 36 % retain tetrahedral coordination. The HDA phase also shows a single N–N bond, which is preserved through both crystallization and decompression processes. At 33 GPa, the majority of atoms (90 % of In and 95 % of N) achieve sixfold coordination, with a minor fraction (6.2 % of In and 1.85 % of N) reaching sevenfold coordination.

Bond angle distribution functions (BADFs) in Fig. 6 provide further insights into structural changes under pressure. For the LDA phase, the bond angle distribution deviates from the ideal tetrahedral angle of 109.47°, showing broad peaks around this value alongside unexpected subpeaks at 88°–90° and larger angles, indicative of local structural motifs like edge-sharing fourfold rings, as observed in nitrogen-based amorphous materials such as $Al_xGa_{1-x}N$ and GaN [23,24]. As pressure increases, the main peak in the BADFs shifts toward smaller angles, reflecting bond geometry distortion. This shift intensifies during the LDA-HDA transformation, where the primary peak centers around 90°, suggesting a significant structural rearrangement. At pressure of 33 GPa, sharper peaks emerge at 90° and 180°, signifying a crystalline-like ordering akin to the RS phase.

To investigate the nature of the LDA-HDA phase transformation, we gradually release pressure from 30 GPa, revealing a clear hysteresis effect (Fig. 1). The recovered model retains its amorphous characteristics, as indicated by the absence of long-range correlations (Fig. 2) and a partial recovery in volume, settling at approximately 4 % greater density than the initial uncompressed structure (see Fig. 1). Coordination analysis shows that in the recovered amorphous structure, approximately 80 % of In atoms and 84 % of N atoms form tetrahedral configurations, while a smaller fraction (~15 %) exhibit fivefold coordination. This leads to an average coordination number of 4.14 for In atoms and 4.16 for N atoms. These results indicate that the recovered model retains some structural motifs from the high-pressure phase. However, since the tetrahedral arrangements largely reestablish themselves, the LDA-HDA transformation in a-InN can be classified as a reversible phase transition.

In Fig.7, we present a comparison of the partial pair distribution functions (PDFs) and bond angle distribution functions (BADFs) of the

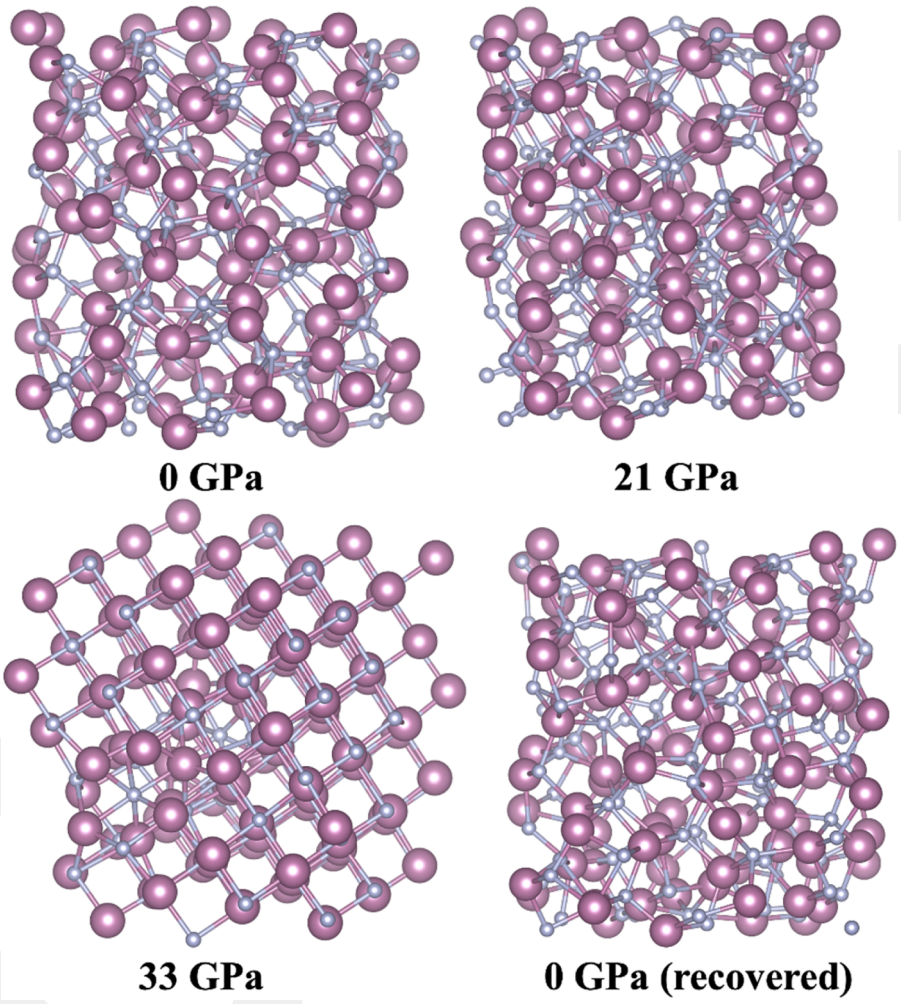


**Fig. 3.** Ball-and-stick models illustrating a-InN structures at different pressure levels.

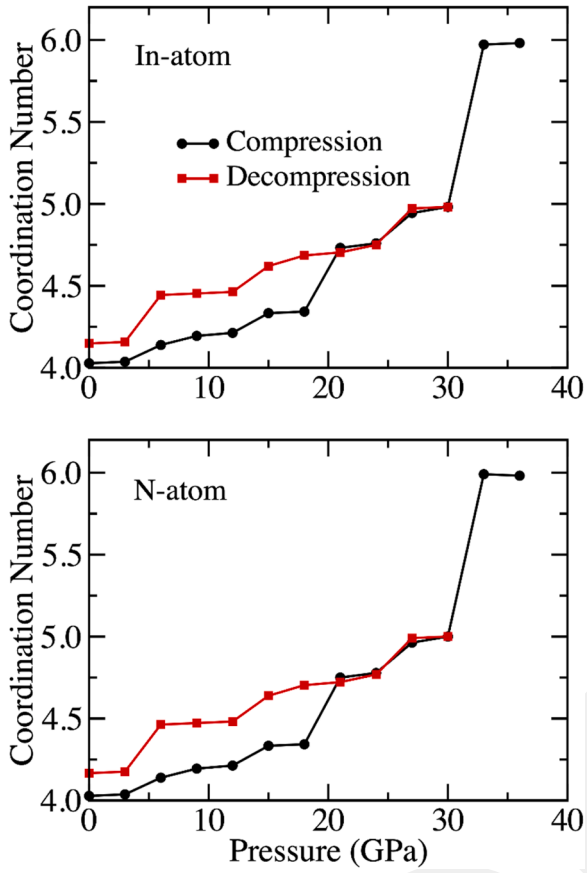


**Fig. 4.** Change in coordination numbers with pressure in a-InN.

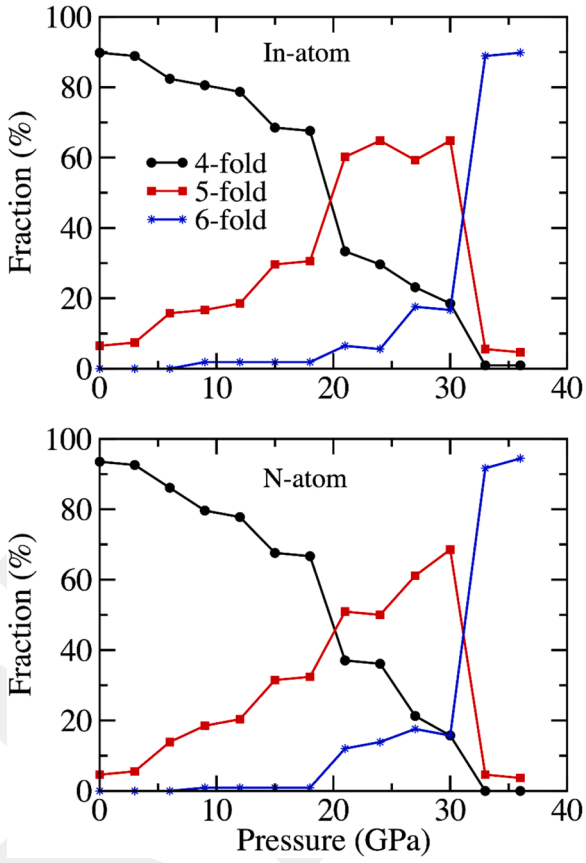


**Fig. 5.** Coordination distribution of a-InN as pressure increases.

uncompressed and recovered models. The first peak in the PDFs for both models is consistently located at 2.17 Å, indicating no significant change in the In-N bond length. However, a slight shift in the second-neighbor peak from 3.523 Å to 3.423 Å is observed in the recovered model, suggesting subtle rearrangements in the intermediate atomic environment.

Analysis of the bond angle distributions reveals no substantial change in the In-N-In bond angle. However, the main peak of the N-In-N distribution shifts slightly to approximately 105° in the recovered model, indicating a minor distortion in the local bonding geometry.

To gain deeper insights into the structural changes, a detailed analysis of the tetrahedral network is conducted using the ISAACS code [25]. Due to the presence of fivefold coordination in the recovered model, a decrease in the total number of tetrahedra is observed. Specifically, the number of tetrahedra reduces from 97 to 87 for In atoms and from 101 to 90 for N atoms. The connectivity of these tetrahedra also exhibits subtle variations. In the uncompressed model, the fractions of corner-sharing and edge-sharing tetrahedra are 91.49 % and 8.51 % for In atoms, and 91.03 % and 8.97 % for N atoms, respectively. In the recovered model, these fractions shift to 96.91 % and 3.09 % for In atoms, and 96.18 % and 3.82 % for N atoms, respectively. This indicates a slight decrease in edge-sharing tetrahedra and a corresponding increase in corner-sharing tetrahedra in the recovered model.

Based on these observations, we conclude that the recovered and uncompressed models are structurally similar, with only minor differences in tetrahedral connectivity and local atomic arrangements. These results suggest that the recovery process preserves the overall structural integrity of the tetrahedral network while introducing slight modifications in bonding topology.

## 4. Discussion

Disordered materials often undergo complex phase transitions under pressure, including amorphous-to-amorphous (LDA-HDA) transitions [26–43] and, in some cases, pressure-induced crystallization [44,45]. The LDA-HDA phase transformation can be either first-order or gradual, with gradual transitions being more commonly observed in amorphous compounds. Under further compression, the HDA phase typically evolves into a very high-density amorphous (VHDA) phase [28,31,42]. In certain cases, such as in AlN [46], crystallization can occur, though it is rare. Continued compression of the VHDA phase may eventually lead to crystallization, following the sequence LDA → HDA → VHDA → crystal [31,32].

In this work, we observe a distinct two-step transformation in a-InN under pressure. Compared to previous high-pressure studies on amorphous compounds, our findings reveal unique behaviors in the high-pressure response of a-InN. First, the first-order nature of the LDA-HDA transition in a-InN is especially notable, as such transitions are rarely observed in typical amorphous compounds. Second, the LDA → HDA → crystal transformation pathway obtained in this study is particularly rare and not commonly encountered in other amorphous materials.

We attribute the first-order amorphous-to-amorphous phase transition and subsequent crystallization of a-InN to the emergence of chemical ordering and the formation of bonding motifs that deviate from the ideal tetrahedral characteristic of the LDA phase. The material's inherent resistance to forming homopolar bonds (In-In and N-N), combined with the presence of specific local structural features, such as edge-sharing units, likely contributes to the observed volume collapses, thereby driving the first-order phase transitions. Additionally, these structural motifs, coupled with pressure-induced changes, appear to play a pivotal role in enabling the transformation from an amorphous to

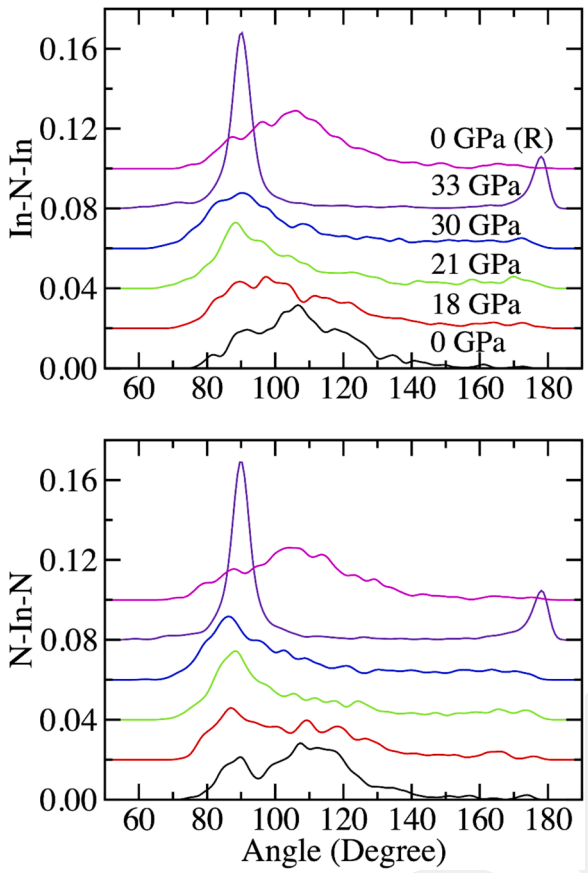


**Fig. 6.** Bond angle distribution function (BADF) of a-InN at selected pressures.

a crystalline phase.

Our simulations suggest that the LDA-HDA transition in a-InN is largely reversible. On decompression, the material returns to an amorphous phase that retains some structural features from the high-pressure states. This persistence may reflect limitations inherent to the simulation process. Consequently, these high-pressure features suggest that the LDA-HDA transition is likely reversible in practice, though experimental confirmation under real-world conditions is necessary to fully understand a-InN's pressure sensitivity.

The Parrinello-Rahman method employed in our simulations is recognized for its tendency to overestimate transition pressures, largely due to certain limitations inherent to the simulation setup. These include the use of periodic boundary conditions, the absence of impurities in our model, and the relatively rapid pressurization rates applied in simulations. Therefore, we anticipate that these phase transformations would likely occur at lower pressures under real-world conditions.

## 5. Conclusion

Our ab initio constant-pressure simulations have revealed the high-pressure phase behavior of a-InN, exposing a distinct two-step transformation under compression. Initially, the LDA phase undergoes a polyamorphic transition to a HDA phase. This HDA structure remains stable within a certain pressure range, and upon further compression, crystallization occurs, resulting in a RS-like structure. Upon decompression, the HDA phase returns to an amorphous state, exhibiting a slightly higher density and coordination number compared to the initial LDA configuration. Notably, the LDA-HDA transition appears to be largely reversible, with the material retaining some features of its high-pressure structure after decompression. These findings highlight several unique behaviors in a-InN's high-pressure response, including the rare occurrence of a first-order LDA-HDA transition and the subsequent

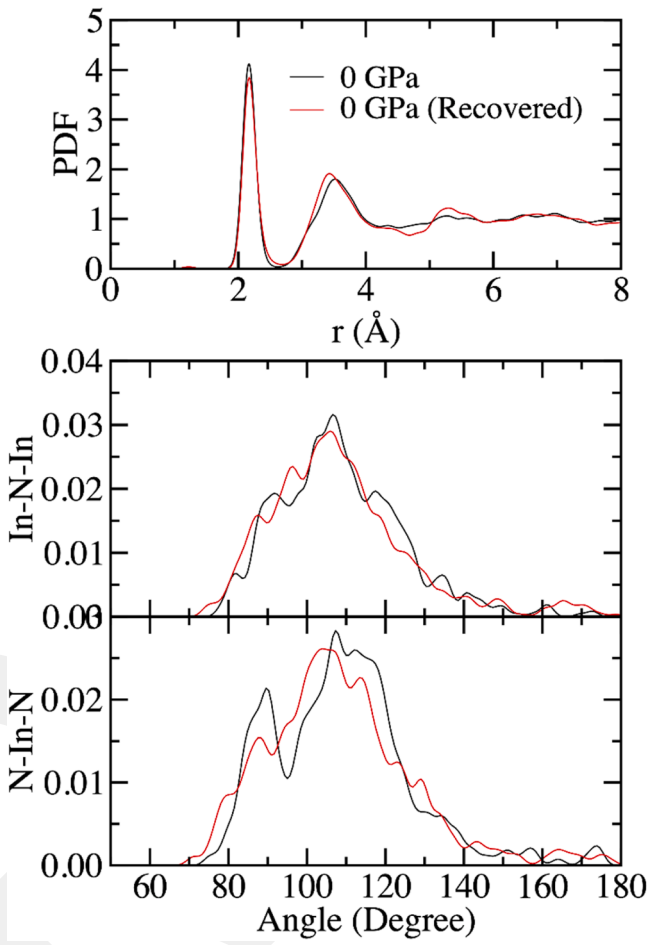


**Fig. 7.** Total pair distribution function (PDF) and bond angle distribution function (BADF) of the uncompressed and recovered amorphous structures of InN.

crystallization into an RS structure, which sets it apart from typical amorphous compounds. While the simulation results provide valuable insights into the pressure-induced structural evolution of a-InN, further experimental studies are needed to confirm the high-pressure response of the material.

### Declaration of generative AI and AI-assisted technologies in the writing process

During the preparation of this work the author(s) used some AI tools in order to improve the language. After using this tool/service, the author(s) reviewed and edited the content as needed and take(s) full responsibility for the content of the publication.

### CRediT authorship contribution statement

**Murat Durandurdu:** Writing – review & editing, Writing – original draft, Visualization, Validation, Methodology, Investigation, Funding acquisition, Formal analysis, Conceptualization.

### Declaration of competing interest

The authors declare that they have no known competing financial interests or personal relationships that could have appeared to influence the work reported in this paper.

## Acknowledgments

The author extends gratitude to the Abdullah Gül University Support Foundation for their support. The author acknowledges the computing resources and time generously provided by TÜBİTAK ULAKBİM High Performance and Grid Computing Center (TRUBA resources).

## Data availability

Data will be made available on request.

## References

[1] V.Y. Davydov, A.A. Klochikhin, R.P. Seisyan, V.V. Emtsev, S.V. Ivanov, F. Bechstedt, J. Furthmüller, H. Harima, A.V. Mudryi, J. Aderhold, O. Semchinova, Absorption and emission of hexagonal InN. Evidence of narrow fundamental band gap, Phys. Status Solidi B 229 (3) (2002) r1–3.
[2] J. Wu, W. Walukiewicz, K.M. Yu, J.W. Ager III, E.E. Haller, H. Lu, W.J. Schaff, Y. Saito, Y Nanishi, Unusual properties of the fundamental band gap of InN, Appl. Phys. Lett. 80 (21) (2002) 3967–3969.
[3] T. Matsuoka, H. Okamoto, M. Nakao, H. Harima, E. Kurimoto, Optical bandgap energy of wurtzite InN, Appl. Phys. Lett. 81 (7) (2002) 1246–1248.
[4] V.W. Chin, T.L. Tansley, T. Osotchan, Electron mobilities in gallium, indium, and aluminum nitrides, J. Appl. Phys. 75 (11) (1994) 7365–7372.
[5] A.G. Bhuiyan, A. Hashimoto, A. Yamamoto, Indium nitride (InN): a review on growth, characterization, and properties, J. Appl. Phys. 94 (5) (2003) 2779–2808.
[6] C.W. Hsu, P. Deminskyi, I. Martinovic, I.G. Ivanov, J. Palisaitis, H. Pedersen, Direct epitaxial nanometer-thin InN of high structural quality on 4H–SiC by atomic layer deposition, Appl. Phys. Lett. 117 (9) (2020).
[7] T. Ernst, C. Chèze, R. Calarco, InN and GaN/InN monolayers grown on ZnO (0001¯) and ZnO (0001), J. Appl. Phys. 124 (11) (2018).
[8] M. Zeghouane, G. Avit, T.W. Cornelius, D. Salomon, Y. André, C. Bougerol, T. Taliercio, A. Meguekam-Sado, P. Ferret, D. Castelluci, E. Gil, Selective growth of ordered hexagonal InN nanorods, CrystEngComm 21 (16) (2019) 2702–2708.
[9] J.M. Khoshman, M.E. Kordesch, Optical absorption in amorphous InN thin films, J. Non Cryst. Solids. 352 (52–54) (2006) 5572–5577.
[10] J.M. Khoshman, M.E. Kordesch, Spectroscopic ellipsometry characterization of amorphous aluminum nitride and indium nitride thin films, Phys. Status Solidi C 2 (7) (2005) 2821–2827.
[11] B. Cai, D.A. Drabold, Ab initio models of amorphous InN, Phys. Rev. B 79 (2009) 195204.
[12] C. Pinquier, F. Demangeot, J. Frandon, J.W. Pomeroy, M. Kuball, H. Hubel, N. W. Van Uden, D.J. Dunstan, O. Briot, B. Maleyre, S. Ruffenach, Raman scattering in hexagonal InN under high pressure, Phys. Rev. B 70 (11) (2004) 113202.
[13] M. Ueno, M. Yoshida, A. Onodera, O. Shimomura, K. Takemura, Stability of the wurtzite-type structure under high pressure: gaN and InN, Phys. Rev. B 49 (1) (1994) 14.
[14] H. Saitoh, W. Utsumi, H. Kaneko, K. Aoki, The phase and crystal-growth study of group-III nitrides in a 2000 °C at 20 GPa region, J. Cryst. Growth 300 (1) (2007) 26–31.
[15] S.V. Ovsyannikov, V.V. Shchennikov, A.E. Karkin, A. Polian, O. Briot, S. Ruffenach, B. Gil, M. Moret, Pressure cycling of InN to 20 GPa: *in situ* transport properties and amorphization, Appl. Phys. Lett. 97 (3) (2010).
[16] J.M. Soler, E. Artacho, J.D. Gale, A. García, J. Junquera, P. Ordejón, Sánchez-Portal D. The SIESTA method for ab initio order-N materials simulation, J. Phys. Condens. Matter 14 (2002) 2745–2779.
[17] D.M. Ceperley, B.J. Alder, Ground state of the electron gas by a stochastic method, Phys. Rev. Lett. 45 (7) (1980) 566–569.
[18] J.P. Perdew, A. Zunger, Self-interaction correction to density-functional approximations for many-electron systems, Phys. Rev. B 23 (10) (1981) 5048–5079.
[19] N. Troullier, J.L. Martins, Efficient pseudopotentials for plane-wave calculations, Phys. Rev. B 43 (1993), 1991.
[20] M. Parrinello, A. Rahman, Polymorphic transitions in single crystals: a new molecular dynamics method, J. Appl. Phys. 52 (1981) 7182–7190.
[21] M. Durandurdu, Uncovering nanoclusters in amorphous AlN: an ab initio study, J. Am. Ceram. Soc. 98 (4) (2015) 1095–1098.
[22] K. Momma, F. Izumi, VESTA 3 for three-dimensional visualization of crystal, volumetric, and morphology data, J. Appl. Crystallogr. 44 (2011) 1272–1276.
[23] B. Cai, D.A. Drabold, Properties of amorphous GaN from first-principles simulations, Phys. Rev. B 84 (2011) 075216–075221.
[24] K. Chen, D.A. Drabold, First principles molecular dynamics study of amorphous Alx_{x}xGa1−x_{1-x}1−xN alloys, J. Appl. Phys. 91 (2002) 9743–9751.
[25] S. Le Roux, V Petkov, ISAACS–interactive structure analysis of amorphous and crystalline systems, J. Appl. Crystallogr. 43 (2010) 81–85.
[26] P.H. Poole, T. Grande, F. Sciortino, et al., Amorphous polymorphism, Comput. Mater. Sci. 4 (1995) 322–373.
[27] O. Mishima, L.D. Calvert, E. Whalley, An apparently first-order transition between two amorphous phases of ice induced by pressure, Nature 314 (1985) 76–78.
[28] R. Martonak, D. Donadio, M. Parrinello, Evolution of the structure of amorphous ice: from low-density amorphous through high-density amorphous to very high-density amorphous ice, J. Chem. Phys. 122 (2005) 134501–134504.
[29] S.K. Deb, M. Wilding, M. Somayazulu, et al., Pressure-induced amorphization and an amorphous–amorphous transition in densified porous silicon, Nature 414 (2001) 528–530.
[30] P.F. McMillan, M. Wilson, D. Daisenberger, et al., A density-driven phase transition between semiconducting and metallic polyamorphs of silicon, Nat. Mater. 4 (2005) 680–684.
[31] V.L. Deringer, N. Bernstein, G. Csányi, C. Ben Mahmoud, M. Ceriotti, M. Wilson, D. A. Drabold, S.R Elliott, Origins of structural and electronic transitions in disordered silicon, Nature 589 (2021) 59–64.
[32] M. Durandurdu, Formation of a very high-density amorphous phase of carbon and its crystallization into a simple cubic structure at high pressure, Comput. Mater. Sci. 200 (2021) 110822–110827.
[33] E. Principi, F. Decremps, A. Di Cicco, et al., Pressure induced phase transitions in amorphous Ge, Phys. Scr. T115 (2005) 381–383.
[34] L. Huang, J. Kieffer, Amorphous-amorphous transitions in silica glass. I. Reversible transitions and thermomechanical anomalies, Phys. Rev. B 69 (2004) 224203.
[35] M. Guerette, M.R. Ackerson, J. Thomas, et al., Structure and properties of silica glass densified in cold compression and hot compression, Sci. Rep. 5 (2015) 15343.
[36] A. Zeidler, K. Wezka, R.F. Rowlands, et al., High-pressure transformation of $SiO_2$ glass from a tetrahedral to an octahedral network: a joint approach using neutron diffraction and molecular dynamics, Phys. Rev. Lett. 113 (2014) 135501–135505.
[37] L. Huang, J. Kieffer, Thermomechanical anomalies and polyamorphism in B2_22O3_33 glass: a molecular dynamics simulation study, Phys. Rev. B 74 (2006) 224107.
[38] P.S. Salmon, J.W. Drewitt, D.A. Whittaker, et al., Density-driven structural transformations in network forming glasses: a high-pressure neutron diffraction study of $GeO_2$ glass up to 17.5 GPa, J. Phys. Condens. Matter 24 (2012) 415102–415117.
[39] V.V. Brazhkin, E. Bychkov, O.B. Tsiok, Direct volumetric study of high-pressure driven polyamorphism and relaxation in the glassy germanium chalcogenides, J. Phys. Chem. B 120 (2016) 358–363.
[40] L. Properzi, A. Di Cicco, L. Nataf, et al., Short-range order of compressed amorphous $GeSe_2$, Sci. Rep. 5 (2015) 10188.
[41] L. Properzi, M. Santoro, M. Minicucci, et al., Structural evolution mechanisms of amorphous and liquid $As_2Se_3$ at high pressures, Phys. Rev. B 93 (2016) 214205–214212.
[42] K. Yoshio, C.Y. Shu, Y.W. Kenney-Benson, G. Shen, Structural evolution of SiO2_{2}2 glass with Si coordination number greater than 6, Phys. Rev. Lett 125 (2020) 205701–205705.
[43] E. Mijit, M. Durandurdu, J.E. Rodrigues, A. Trapananti, S.J. Rezvani, A.D. Rosa, O. Mathon, T. Irifune, A. Di Cicco, Structural and electronic transformations of $GeSe_2$ glass under high pressures studied by X-ray absorption spectroscopy, Proc. Natl. Acad. Sci. U. S. A. 121 (14) (2024).
[44] M. Xu, Y. Meng, Y.Q. Cheng, H.W. Sheng, X.D. Han, E. Ma, Pressure-induced crystallization of amorphous $Ge_2Sb_2Te_5$, J. Appl. Phys. 108 (2010) 083519–083523.
[45] M. Wu, J.S. Tse, S.Y. Wang, C.Z. Wang, J.Z. Jiang, Origin of pressure-induced crystallization of $Ce_{75}Al_{25}$ metallic glass, Nat. Commun. 6 (2015) 6493–6649.
[46] M. Durandurdu, Polyamorphism in aluminum nitride: a first-principles molecular dynamics study, J. Am. Ceram. Soc. 99 (2016) 1594–1600.